International Journal of Nanomedicine

Dovepress
open access to scientific and medical research

Open Access Full Text Article

ORIGINAL RESEARCH

SERS Analysis Platform Based on Aptamer Recognition-Release Strategy for Efficient and Sensitive Diagnosis of Colorectal Precancerous Lesions

Fengsong Chen[1,*], Yanhua Huang[1,*], Yongxia Liu[2], Yanwen Zhuang[3], Xiaowei Cao[3], Xiaogang Qin[2]

[1]Department of Gastroenterology, Nantong Haimen People's Hospital, Nantong, Jiangsu, 226100, People's Republic of China; [2]Department of gastroenterology, Traditional Chinese Medicine Hospital of Tongzhou District, Nantong, Jiangsu, 226300, People's Republic of China; [3]Institute of Translational Medicine, Medical College, Yangzhou University, Yangzhou, Jiangsu, 225001, People's Republic of China

*These authors contributed equally to this work

Correspondence: Xiaogang Qin, Email tzqinxiaogang@163.com

Background: Colorectal cancer (CRC) has become a significant global public health challenge, demanding immediate attention due to its high incidence and mortality rates. Regular CRC screening is essential for the early detection of precancerous lesions and CRC.

Methods: : We developed a novel surface-enhanced Raman scattering (SERS) analysis platform that employs high-throughput microarray chips as carriers and Au/SnO_2 nanoring arrays (Au/SnO_2 NRAs) as substrates. This platform utilizes an aptamer recognition-release strategy to achieve efficient and sensitive detection of protein tumor markers. In the detection process, the strong affinity and high specificity between the aptamer and the target protein result in competitive replacement of the SERS nanoprobes originally bound to the substrate surface. As a result, the SERS nanoprobes carrying Raman reporter genes are dislodged, leading to a reduction in the SERS signal intensity.

Results: The platform demonstrated excellent detection performance, with rapid detection completed within 15 minutes and limits of detection (LOD) as low as 6.2×10^{-12} g/mL for hnRNP A1 and 6.51×10^{-12} g/mL for S100P. Clinical samples analyzed using the SERS platform showed high consistency with enzyme-linked immunosorbent assay (ELISA) results.

Conclusion: This platform offers strong support for the early detection, risk assessment, and treatment monitoring of colorectal cancer precancerous lesions, with broad potential for clinical applications.

Keywords: colorectal cancer, precancerous lesions, surface enhanced raman scattering, aptamer, microarray chip

Introduction

Colorectal cancer (CRC) is one of the most prevalent malignant tumors of the gastrointestinal tract.[1] Due to the lack of distinct early symptoms, CRC is often overlooked by patients, leading to a majority being diagnosed at advanced stages.[2] The high morbidity and mortality rates associated with CRC pose a significant threat to human health and life.[3,4] Detecting and intervening in precancerous lesions at an early stage is crucial for improving the survival rate of CRC patients.[5] Currently, traditional methods, such as colonoscopy, are challenging to implement on a large scale in the general population due to their invasiveness, the complexity of the instrumentation, intricate procedures, and patient intolerance.[6] In recent years, multi-targeted fecal DNA testing has emerged as a non-invasive CRC screening method. It has gained popularity due to its non-invasiveness, painlessness, safety, and convenience. However, it remains hindered by high costs and low specificity.[7,8] Thus, the search for novel CRC biomarkers and diagnostic tools has become a key focus in current research.[9–11] For instance, Lee et al developed a surface plasmon resonance biosensor based on heterogeneous nuclear ribonucleoprotein A1 (hnRNP A1), which was used to analyze plasma samples for CRC.[12] Shen's team identified

Received: 12 August 2024
Accepted: 18 September 2024
Published: 30 September 2024

elevated expression of S100 calcium-binding protein P (S100P) in CRC patient tissues, finding it to be closely associated with CRC invasiveness and metastasis.[13] hnRNP A1 and S100P have both been proposed as potential diagnostic biomarkers for CRC.

Several detection methods for protein biomarkers have been extensively reported, including enzyme-linked immunosorbent assay (ELISA), immunohistochemistry (IHC), and mass spectrometry analysis.[14–16] However, these methods are often hindered by complex operations and poor accuracy, making them unsuitable for large-scale sample analysis.[17] Surface-enhanced Raman spectroscopy (SERS) is a vibrational fingerprint spectroscopy technique known for its extremely high sensitivity and accuracy.[18] SERS enhances weak Raman signals by utilizing surface nanostructures and surface plasmon resonance effects, allowing for the precise detection of trace compounds.[19] It holds great potential in the detection and analysis of body fluids, due to its resilience to water interference, fast response, and non-destructive analysis.[20–22] Compared to traditional sandwich-based strategies that require two incubation cycles, SERS technology, combined with an aptamer-based recognition-release detection strategy, has gained attention for protein biomarker detection. This approach is recognized for its high specificity, strong affinity, low cost, and simple and rapid operation.[23,24]

Although SERS has demonstrated significant potential in protein biomarker detection, its clinical application is still largely constrained by challenges such as high sample consumption and poor reproducibility during the detection process.[25–27] Addressing the preparation of structurally stable, hotspot-dense, and uniformly distributed SERS substrates is an urgent issue. Au/SnO_2 nanoring arrays (Au/SnO_2 NRAs) consist of uniformly sized, regularly arranged ring structures in close contact. Due to their rough surface and narrow nanogaps between particles, Au/SnO_2 NRAs offer high strength and reproducibility in SERS enhancement. As an integrated chip platform, microarray chips present several advantages, including high throughput, low sample consumption, improved safety, and a small, portable structure. These characteristics enable simple and rapid sample detection.[28–31] In recent years, the combination of SERS technology and microarray chips has gained increasing attention from researchers, bringing new vitality to fields such as biological detection and medical diagnosis.[32–34]

In this study, we developed a novel high-throughput SERS analysis platform based on an aptamer recognition-release strategy by integrating SERS technology with the advantages of microarray chips. This platform enables the high-sensitivity recognition and rapid detection of colorectal precancerous lesion biomarkers, hnRNP A1 and S100P. We constructed Au/SnO_2 NRAs with the tight contact ring structures, consisting of rough rings arranged in a highly ordered pattern and with controllable sizes, resulting in excellent SERS enhancement effects. SnO_2 offers good biocompatibility and is easily modified chemically (Figure 1B). Following this, we synthesized Au nanocube particles (AuNCs) and modified them with Raman reporter genes (4-MBA and DTNB) and aptamer complementary strands (cDNA1 and cDNA2), creating two types of SERS nanoprobes (Figure 1A). The novel SERS sensor was successfully constructed by combining the SERS nanoprobes with complementary bases in the aptamer chain and fixing them on the Au/SnO_2 NRA substrate. When the target proteins, hnRNP A1 and S100P, are present, the aptamer's affinity for the target protein far exceeds that of the complementary chains (cDNA1 and cDNA2), causing the SERS probe with the Raman reporter gene to detach competitively. This results in a significant decrease in the SERS signal intensity of the characteristic peak (Figure 1C). Finally, the detection results obtained from clinical samples using the SERS analysis platform were compared and analyzed against those from the widely used enzyme-linked immunosorbent assay (ELISA). The SERS platform accurately met the detection requirements for protein tumor markers (hnRNP A1 and S100P) in clinical blood samples. In conclusion, this novel SERS microarray chip, utilizing the aptamer recognition-release strategy, not only offers a new perspective for clinical biomarker detection but also provides innovative approaches for screening CRC.

Materials and Methods

Materials

Cetyltrimethylammonium chloride (CTAC), sodium borohydride ($NaBH_4$), ascorbic acid (AA), polyethylene glycol (PEG), tin tetrachloride ($SnCl_4$), 5,5′-dithiobenzoic acid (2-nitrobenzoic acid) (DTNB), and 4-mercaptobenzoic acid (4-MBA) were obtained from Nanjing Chemical Reagent Co. Chloroauric acid ($HAuCl_4$), polydimethylsiloxane (PDMS), anhydrous ethanol, and phosphate buffer salt (PBS) were supplied by Shanghai Jizi Biochemical Technology Co. A monodisperse polystyrene (PS)

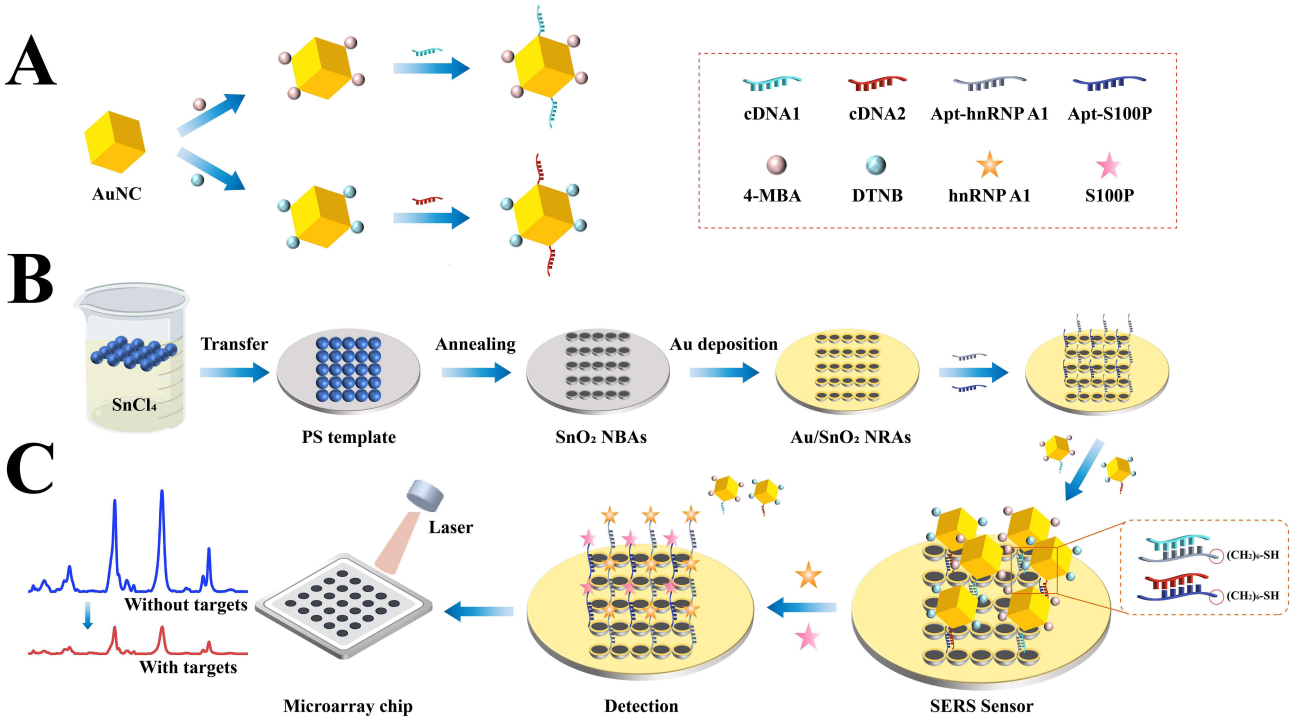

Figure 1 (**A**) Synthesis of SERS nanoprobes. (**B**) Construction of SERS sensors. (**C**) SERS analysis platform using microarray chips as carriers.

microsphere solution (5 wt%) with a diameter of 500 nm was sourced from Beijing Zhongke Keyou Technology Co. The human hnRNP A1 enzyme immunoassay kit (GOY-(elisa)-12236) was purchased from Shanghai Guyan Industrial Co., while the human S100P enzyme immunoassay kit (ab314385) was acquired from Abcam, UK. Aptamers and nucleotide sequences used in the experiments (Table 1) were synthesized by Sangon Bioengineering (Shanghai) Co. Deionized water used in all experiments was purified using a microtiter Milli-Q system (18.2 MΩ cm^{-1}).

Instrumentation

Ultraviolet-visible-near infrared (UV-vis-NIR) absorption spectra were measured using a UV-vis spectrophotometer (Cary 60, Agilent). Scanning electron microscopy (SEM) images were captured using an S-4800 II field emission scanning electron microscope, while transmission electron microscopy (TEM) images were obtained using a JEM-2100 transmission electron microscope. High-resolution, localized images of the nanomaterials were observed with the Tecnai F30 field emission high-resolution transmission electron microscope. SERS spectra were acquired using a Renishaw inVia laser Raman spectrometer.

Clinical Specimens

Human blood samples were collected from the Traditional Chinese Medicine Hospital of Tongzhou District, with approval from the Ethics Committee. Based on the diagnostic criteria provided by the Chinese Diagnostic and

Table 1 Nucleotide Sequences Used in the Experiment

Name	Sequences (5′ −3′)
Apt-hnRNP A1	-SH-$(CH_2)_6$-GCA ATG GTA CGG TAC TTC CTG TGG CGA GGT AGG TGG GGT GTG TGT GTA TCC AAA AGT GCA CGC TAC TTT GCT AA
Apt-S100P	-SH-$(CH_2)_6$-ATC CAG AGT GCA GCA GGA CTG CTT AGG ATT GCG AAG TGC ATA GAG CGG CTA TGG ACA CGG TGG CTT AGT
cDNA1	-SH-CTA CCC CAC CTA CCT CGC CAC AGG AAG TAC CGT ACC ATT GCA
cDNA2	-SH-CAA ATC CTA AGC AGT CCT GCT GCA CTC TGG ATG

Therapeutic Criteria for Colorectal Cancer (Version 2023), a total of 90 human subjects participated: 30 healthy individuals, 30 patients diagnosed with CRC precancerous lesions by pathological examination, and 30 patients with CRC. All participants signed informed consent forms. Blood samples were collected on the same day and processed according to standard operating procedures (SOPs). The obtained serum samples were stored at −80°C. Detailed information regarding the 90 subjects is provided in Table S1.

Synthesis of AuNCs

In brief, AuNCs were synthesized using a seed growth method. Initially, HAuCl solution (0.01 M, 0.25 mL) was added to CTAC solution (0.1 M, 7.5 mL) and thoroughly mixed. While continuously stirring, freshly prepared iced $NaBH_4$ solution (10 mM, 0.6 mL) was quickly added. The mixture was stirred vigorously for 2 minutes and then allowed to stand at room temperature for two hours to form the seed solution. The growth solution was prepared by mixing CTAC solution (0.1 M, 3 mL), $HAuCl_4$ solution (0.01 M, 0.5 mL), AA solution (0.1 M, 2 mL), and deionized water (15 mL). After mixing well, the seed solution was diluted to 1/10 of its original concentration, and 10 μL of the diluted seed solution was added to the growth solution. The mixture was gently stirred and then left at room temperature for 24 hours. The final product was washed and centrifuged twice, and then resuspended in deionized water for later use.

Synthesis of Au/SnO_2 NRAs

Polystyrene (PS) microspheres were transferred and immersed in $SnCl_4$ reaction solution at a concentration of 0.05 M. PS monolayer arrays were obtained through a self-assembly process. After annealing at 400°C for 2 hours, flat, bowl-shaped tin oxide structures (SnO_2 NBAs) were formed. The SnO_2 NBAs were then subjected to Au deposition using a magnetron sputtering process with the following parameters: a current of 30 mA, a deposition time of 8 minutes, and an equivalent deposition thickness of 180 nm. After Au deposition, closely packed, ordered Au/SnO_2 NRAs were formed.

Preparation of SERS Nanoprobes

To label AuNCs with signal molecules, 4-MBA and DTNB were selected and bound to AuNCs via Au-S covalent bonding. The process involved adding 8 mL of AuNCs solution and 200 μL of 4-MBA solution (5 mM) to a 25 mL beaker and stirring vigorously for 1 hour to obtain AuNCs@4-MBA. Subsequently, freshly prepared TCEP buffer (5 μL, 50 mM) was used to activate the terminal sulfhydryl groups of cDNA1. The activated cDNA1 solution was slowly added to the AuNCs@4-MBA solution and incubated for 2 hours at 37°C, allowing cDNA1 to form stable gold-sulfur bonds with the gold atoms on the surface of the AuNCs through its active sulfhydryl groups. Finally, 15 μL of BSA solution (1% wt) was added, reacting for 2 hours. After purification by centrifugation, the solution was resuspended in PBS to obtain AuNCs@4-MBA@cDNA1. The same procedure was followed to synthesize AuNCs@DTNB@cDNA2.

Construction of SERS Sensor

Freshly prepared TCEP buffer-activated Apt-hnRNP A1 and Apt-S100P solutions (0.1 mM) were conjugated to the surface of the synthesized Au/SnO_2 NRAs. After incubation at 37°C for 2 hours, the unbound aptamers were removed by rinsing with PBS buffer. The prepared SERS nanoprobes were then added dropwise to the modified Au/SnO_2 NRAs substrate surface, incubated at 37°C for 1.5 hours, and subsequently rinsed with PBS buffer. This completed the preparation of the SERS sensor.

Preparation of Microarray Chip

The microarray chip's size, shape, and distribution were designed using AutoCAD software to ensure compatibility with experimental requirements. A microarray mold was constructed using soft lithography. SU-8 was spin-coated onto a cleaned silicon wafer, followed by curing, exposure, and development to create the microarray mold. Next, the vacuum-treated PDMS mixture (PDMS agent=10:1) was poured into the molds, vacuum-treated again, and cured in an oven at 80°C for 3 hours. After cooling to room temperature, the PDMS chips were punched according to the design, cleaned using an ultrasonic machine, and dried to obtain stable PDMS microarray chips. Finally, the dried PDMS chips and slides were surface-modified to increase the hydrophilicity of the PDMS chip surface.

SERS Measurement

The sample solution for testing was prepared by mixing equal volumes of gradient concentrations of hnRNP A1 and S100P. A 15 μL aliquot of the sample solution was added dropwise to the microarray chip, and the reaction was allowed to proceed at room temperature for 15 minutes. SERS detection was then performed using the Renishaw InVia Laser Raman Spectrometer, with the following parameters: 50× objective lens, 785 nm laser wavelength, 5 mW power, and a data acquisition time of 5 seconds. To ensure data reliability, the spectra for each sample were averaged from 5 randomly selected points within the reaction area. The data were pre-processed using Origin 2021 software for baseline correction and spectral smoothing to facilitate further analysis.

Statistical Analysis

SPSS 27.0 software was used for statistical analysis. Metric data following a normal distribution were expressed as mean ± standard deviation ($\bar{x} \pm s$). Count data were presented as n. A chi-square test was used to assess whether gender was associated with disease progression (healthy, precancerous lesions, CRC). One-way ANOVA was employed to determine if there were significant differences in average age among the three groups. $P < 0.05$ was considered statistically significant.

Results

Characterization of AuNCs

The morphology of the SERS nanoprobes was characterized using electro-optical techniques. SEM images (Figure 2A) revealed that the AuNCs exhibited a regular hexahedral structure with uniform size, and an average edge length of 68 nm. TEM images (Figure 2B) and HRTEM images (Figure 2C) further confirmed that the AuNCs had sharp edges and corners, as well as a high specific surface area. This structural composition allows AuNCs to demonstrate an excellent localized surface plasmon resonance (LSPR) effect and facilitates various chemical modifications. In the locally magnified image of an AuNC (Figure 2D), the lattice spacing of the AuNC was measured to be 0.236 nm, which corresponds to the theoretical value of the {111} lattice plane of the Au crystal structure. Figure 2E shows the changes in UV-vis absorption spectra during the

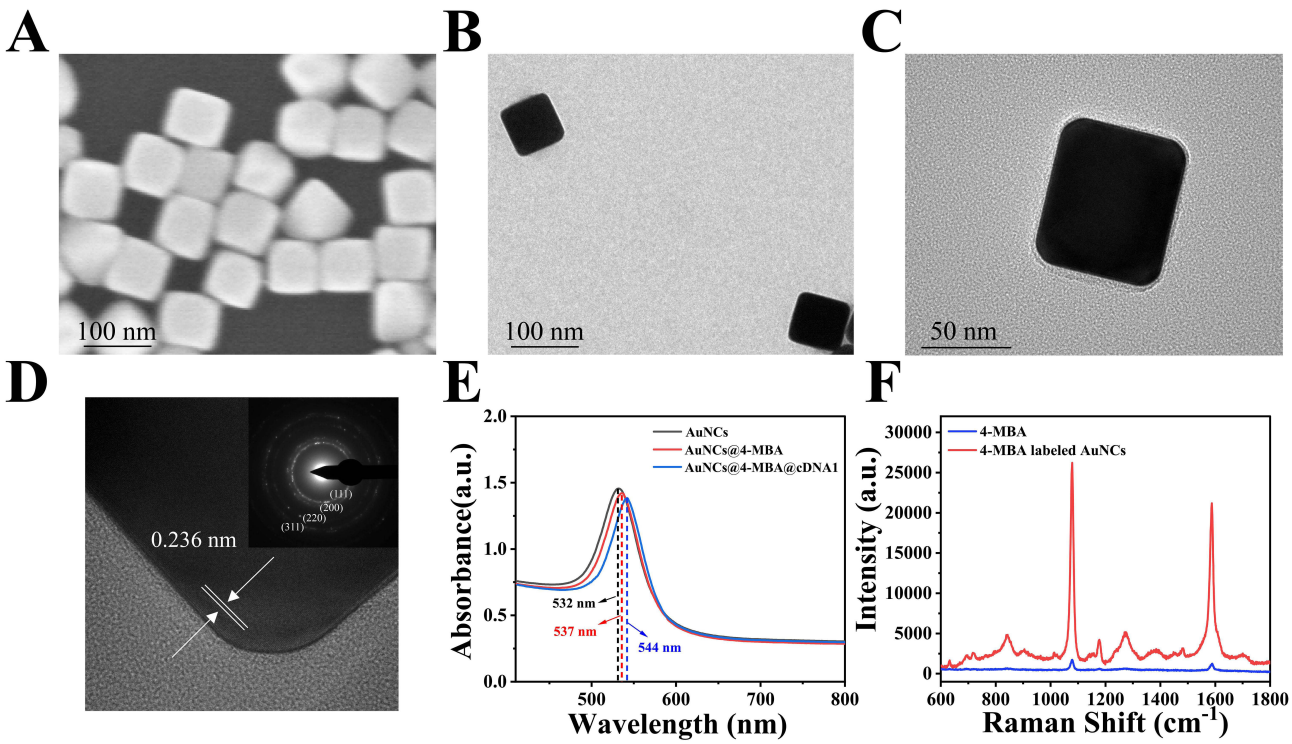

Figure 2 (**A**) SEM image, (**B**) TEM image and (**C**) HRTEM image of AuNCs. (**D**) Localized magnified image and SAED mode image of AuNCs. (**E**) Ultraviolet-visible absorption spectra of SERS probe preparation process. (**F**) Raman spectra of pure 4-MBA and 4-MBA-labeled AuNCs.

preparation of AuNCs@4-MBA@cDNA1. As the 4-MBA and cDNA1 were gradually modified onto the AuNC surface, the maximum absorption peak red-shifted from 532 nm to 544 nm, while the intensity of the absorption peak slightly decreased. These spectral changes were attributed to the interaction between the surface modifiers and the AuNCs' plasma, which altered the electronic environment near the surface and affected light absorption efficiency. Additionally, the SERS activity of the AuNCs was evaluated using the characteristic peak intensity of 4-MBA at 1078 cm^{-1} (Figure 2F). Based on the formula for the enhancement factor (EF): $EF= (I_{SERS}/C_{SERS})/(I_{Raman}/C_{Raman})$,[35] and when $C_{Raman} = 10^{-1}$ M, $C_{SERS} = 10^{-5}$ M, the value of EF is 1.52×10^{5}. AuNCs have excellent SERS enhancement.

Characterization of Au/SnO_2 NRAs

The morphological changes during the preparation of Au/SnO_2 NRAs were characterized. PS microspheres (500 nm in diameter) submerged in a low concentration of $SnCl_4$ solution were self-assembled onto hydrophilic-treated wafers via the gas-liquid interface (Figure 3A). The resulting arrangement exhibited a highly ordered pattern, forming a strong foundation for the subsequent preparation of size-controllable Au/SnO_2 NRAs. SEM images of the intermediate product SnO_2 NBAs, are shown in Figure 3B, where the PS microsphere arrays display flat, bowl-shaped tin oxide structures following annealing. Figure 3C and D present SEM images of Au/SnO_2 NRAs at different magnifications. The flat-

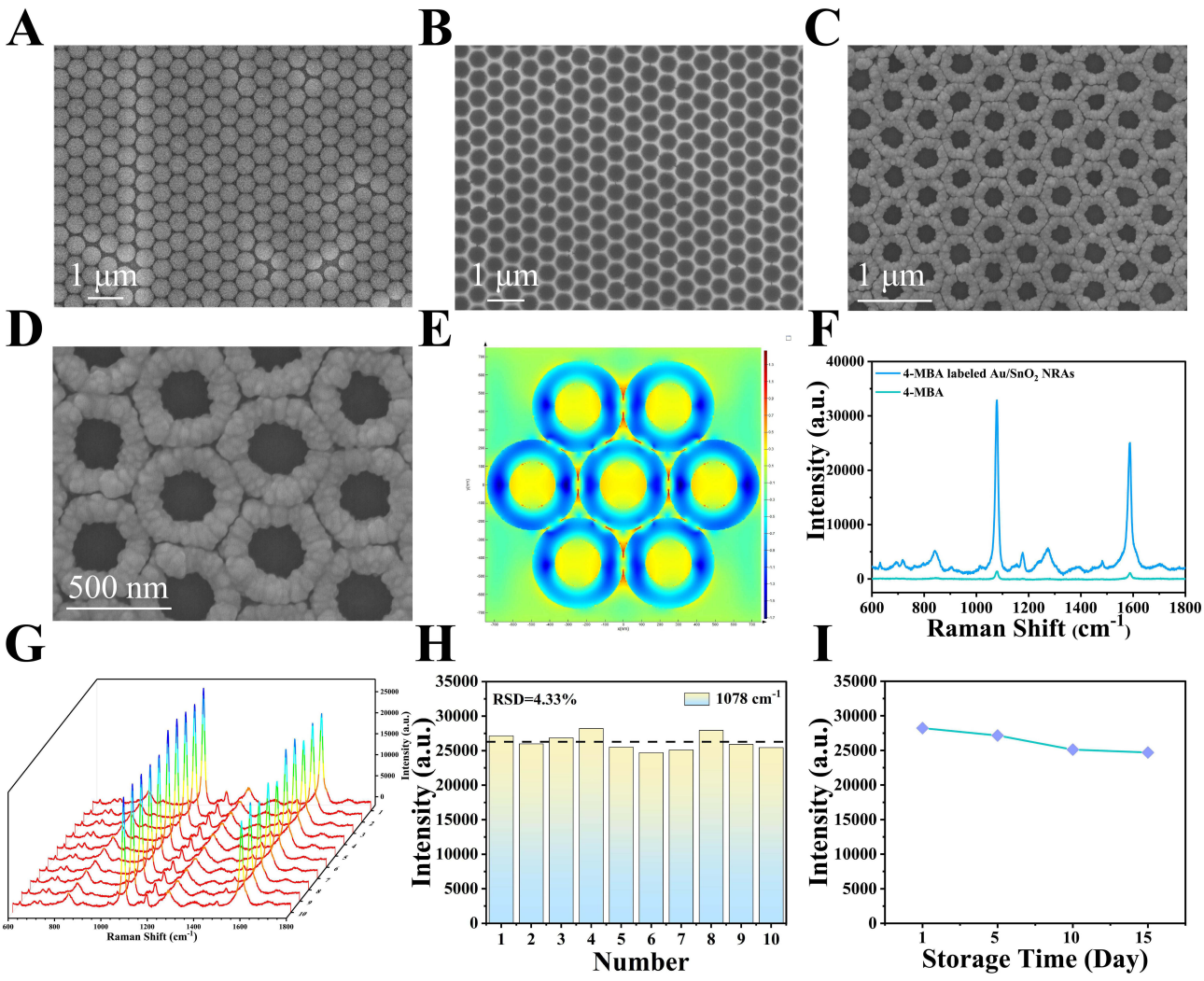

Figure 3 (**A**) SEM images of neatly ordered PS microsphere monolayer templates. (**B**) SEM images of SnO_2 NBAs. (**C**) SEM images of Au/SnO_2 NRAs at low magnification and (**D**) high magnification. (**E**) Electromagnetic field simulation images of Au/SnO_2 NRAs. (**F**) Raman spectra of pure 4-MBA and 4-MBA-labeled Au/SnO_2 NRAs. (**G**) Full SERS spectra of any 10 points on the surface of the 4-MBA-labeled Au/SnO_2 NRAs array and (**H**) histogram of the intensity of Raman characteristic peaks at 1078 cm^{-1}. (**I**) Folded line plots of the intensity of Raman characteristic peaks at 1078 cm^{-1} of 4-MBA-labeled Au/SnO_2 NRAs arrays under different days of storage at room temperature.

mouthed, bowl-shaped SnO_2 NBAs transform into regularly arranged peripheral annular structures after Au deposition, forming Au/SnO_2 NRAs. To understand the electric field intensity distribution of Au/SnO_2 NRAs, a 3D model of the structures was developed and simulated (Figure 3E). The SERS activity of Au/SnO_2 NRAs was evaluated using 4-MBA labeling and SERS spectroscopy (Figure 3F). The EF was calculated to be 2.53×10^8 when $C_{Raman} = 10^{-1}$ M and $C_{SERS} = 10^{-8}$ M, indicating the significant SERS enhancement properties of Au/SnO_2 NRAs. Ten points were randomly selected on the surface of the 4-MBA-labeled Au/SnO_2 NRAs for SERS spectroscopy (Figure 3G), and the Raman characteristic peak at 1078 cm^{-1} was plotted as a histogram of spectral intensity (Figure 3H). The relative standard deviation (RSD) was 4.33%, demonstrating excellent signal homogeneity across the surface of Au/SnO_2 NRAs. Finally, the stability of the Au/SnO_2 NRAs was assessed by performing SERS measurements on samples stored at room temperature for different periods (1, 5, 10, and 15 days). The intensity of the Raman characteristic peak at 1078 cm^{-1} was plotted as a line graph (Figure 3I), with an RSD of 5.49%, indicating that the Au/SnO_2 NRAs possess good stability over time.

Experimental Parameters Optimization

To improve the detection performance of the SERS analysis platform, we optimized key experimental parameters, including cDNA concentration, temperature, and incubation time. The Raman characteristic peaks at 1073 cm^{-1} (4-MBA) and 1330 cm^{-1} (DTNB) were used to assess the SERS intensity changes under various conditions. As shown in Figure 4A, SERS intensities at 1073 cm^{-1} and 1330 cm^{-1} increased with rising cDNA concentrations, stabilizing when the cDNA concentration reached 1 μM, indicating that the coupled cDNA had approached saturation. Therefore, 1 μM was identified as the optimal cDNA concentration for the SERS analysis platform. Temperature and incubation time also significantly influenced detection efficiency. As illustrated in Figure 4B, SERS intensity increased with temperature, but began to decrease once the temperature exceeded 37°C, suggesting that this is the optimal temperature for the reaction. Similarly, Figure 4C shows that SERS intensities at 1073 cm^{-1} and 1330 cm^{-1} decreased with increasing incubation time, stabilizing at 15 minutes. This trend is attributed to the competitive displacement of the SERS nanoprobes carrying signal molecules by the target samples, resulting in a reduction of SERS signal intensity.

Performance Assessment

Evaluating the specificity, reproducibility, and stability of SERS analytical platforms is crucial to improving the accuracy and reliability of detection results. To effectively differentiate targets from non-target analytes, we assessed the specificity of the platform. The blank sample was used as a control, with CEA and AFP as interferents, and the individual target and combined target as the target group (1×10^{-7} g/mL). The Raman spectra for the blank, CEA, and AFP groups showed no significant changes, whereas the SERS intensity of the corresponding characteristic peaks significantly decreased in the presence of the target (Figure 5A). Histograms of the corresponding SERS intensities at 1073 cm^{-1} and 1330 cm^{-1} (Figure 5B) provide a clearer view: compared to the control and interferent groups, the average SERS intensity at 1073 cm^{-1} in the target group decreased by 76.43%, and the average intensity at 1330 cm^{-1} decreased by 76.67%. This

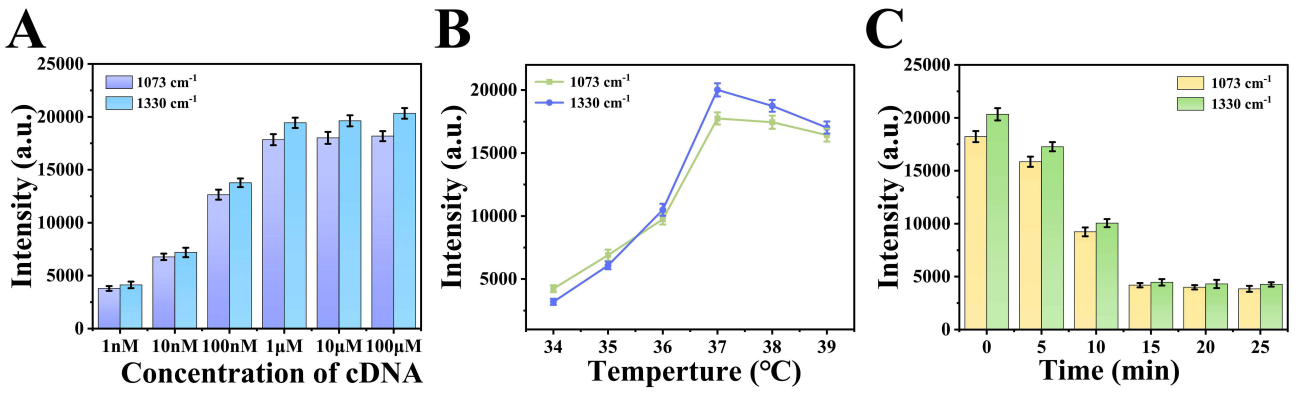

Figure 4 Optimization of reaction conditions: optimization of (**A**) concentration of cDNA, (**B**) temperature and (**C**) incubation time.

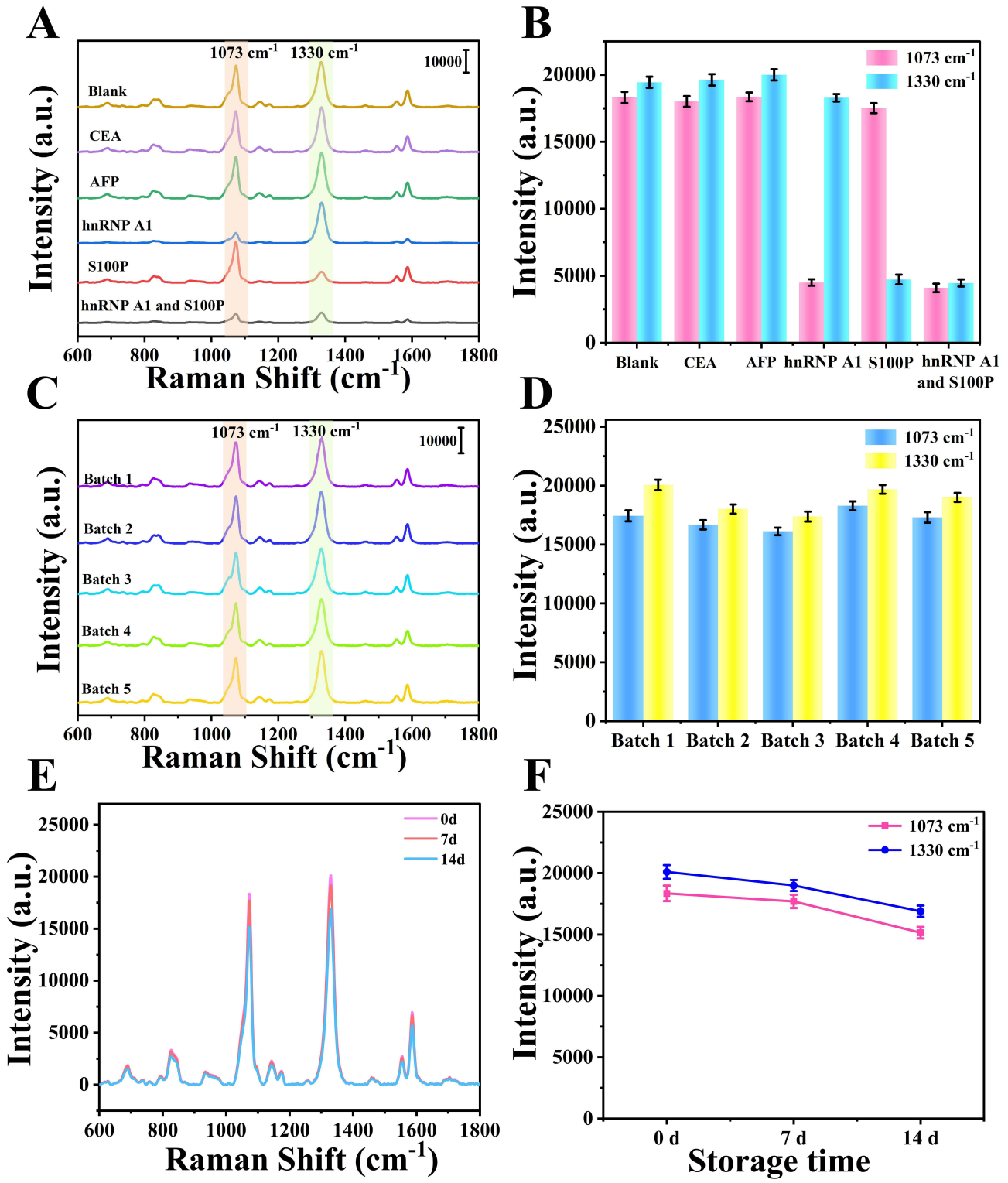

Figure 5 Microarray chip as the SERS analysis platform for performance evaluation: (**A**) specificity assessment and (**B**) histogram corresponding to SERS intensity at 1073 cm^{-1} and 1330 cm^{-1}. (**C**) Reproducibility assessment and (**D**) histogram corresponding to SERS intensity at 1073 cm^{-1} and 1330 cm^{-1}. (**E**) Storage stability assessment and (**F**) line plots corresponding to SERS intensity at 1073 cm^{-1} and 1330 cm^{-1}.

confirms that the integrated microarray platform for SERS analysis can accurately distinguish the target from interferences with excellent specificity. Reproducibility is another critical factor affecting the reliability of microarray chip detection results. As shown in Figure 5C and D, five batches of SERS microarray chips were prepared at different times

and subjected to SERS detection. The results showed no significant differences, with RSD values of 5.19% and 5.96% for SERS intensities at 1073 cm^{-1} and 1330 cm^{-1}, respectively. This demonstrates the excellent reproducibility of the integrated chip as a platform for SERS analysis. Lastly, we assessed the storage stability of the platform. SERS microarray chips were stored at room temperature for 0, 7, and 14 days, and their SERS spectra were recorded to evaluate stability. As shown in Figure 5E, no significant changes in the shape of the SERS curves were observed, with only minor variations in intensity. The intensity variations at 1073 cm^{-1} and 1330 cm^{-1} are shown in Figure 5F, with RSD values of 7.03% and 7.17%, respectively, confirming the platform's significant stability. Additionally, the platform exhibited good reproducibility (Figure S1), with RSD values of 5.29% and 6.52% for SERS intensities at 1073 cm^{-1} and 1330 cm^{-1}, respectively.

Quantitative Determination

Following the optimization of experimental parameters and performance evaluation, sensitivity remains a key factor for the SERS analytical platform. Serum sample solutions containing a 1:1 mixture of hnRNP A1 and S100P were prepared in various concentrations (10^{-12} to 10^{-6} g/mL), and the SERS platform was employed for simultaneous quantitative detection of these biomarkers. The SERS intensities at 1073 cm^{-1} and 1330 cm^{-1} decreased significantly as the concentration increased (Figure 6A). This is due to the strong specificity and affinity between the aptamer and the target, which results in the displacement of the SERS nanoprobes carrying the signaling molecules, leading to a reduction in SERS signal intensity. As shown in Figure 6B and C, the logarithm of target concentration displayed a strong linear correlation with SERS intensity. The standard curve equations were y = −2688.67x −14642.47 (R^2 = 0.9843) for hnRNP A1 and y = −2980.61x −16112.55 (R^2 = 0.9836) for S100P. The limits of detection (LOD) were determined to be 6.2×10^{-12} g/mL for hnRNP A1 and 6.51×10^{-12} g/mL for S100P. When compared with other assays (Table 2), the SERS technology combined with the microarray chip demonstrated a wider detection range and superior sensitivity, with the added advantage of a very short assay time. Results were obtained within just 15 minutes. The SERS analytical platform developed in this study exhibits significant potential for use in the diagnosis and screening of colorectal precancerous lesions.

Characterization of Clinical Samples

Clinical samples were obtained from the Traditional Chinese Medicine Hospital of Tongzhou District. The diagnosis of CRC involves a thorough and systematic process to ensure accurate and comprehensive results. As shown in Figure 7A, D, and G, colonoscopy of healthy individuals revealed smooth intestinal mucosa with clear vascular texture. Imaging showed normal intestinal wall thickness, with no evidence of thickening or mass. Pathological analysis indicated intact intestinal mucosal tissue with neatly arranged cells and no anisotropy. In contrast, Figure 7B, E, and H depict an elevated lesion in the rectum, with uneven surface mucosa and nodular hyperplasia. The intestines showed poor demarcation from adjacent structures such as the liver and pancreas. Pathological examination confirmed the presence of a choriocapillary-tubular adenoma with high-

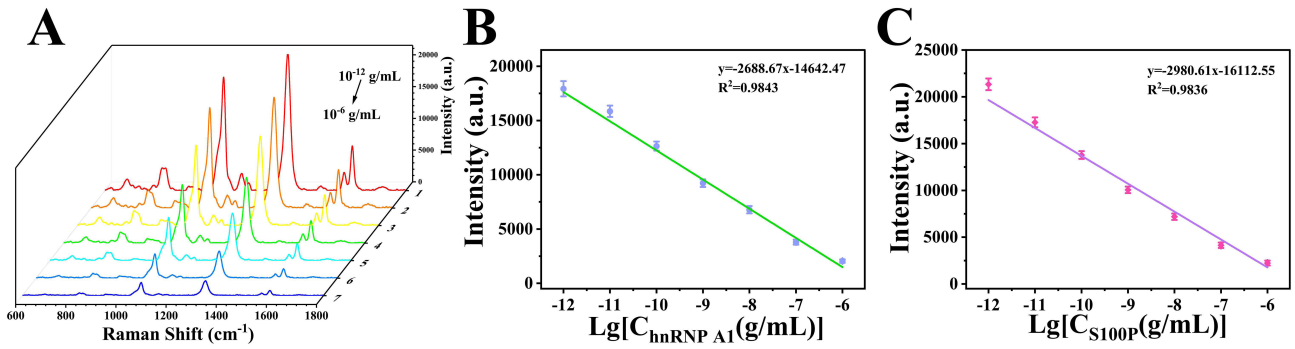

Figure 6 (**A**) SERS spectra of different concentrations of hnRNP A1 and S100P (hnRNP A1: S100P=1:1) in serum. (**B**) Calibration curve of the logarithmic correlation between the intensity of the characteristic peak at 1073 cm^{-1} and the concentration of hnRNP A1. (**C**) Calibration curve of the characteristic peak intensity at 1330 cm^{-1} related to the logarithm of S100P concentration.

Table 2 Comparison Between the SERS Analytics Platform Proposed in This Work and Other Methods in Biomarkers Detection

Detection method	Biomarker	Linear Range	LOD	Time	Reference
Electrochemistry	CEA	1×10^{-8}-2.5×10^{-7} g/mL	8.6×10^{-9} g/mL	45 min	[36]
Fluorescence	AFP	4×10^{-8}-6.4×10^{-7} g/mL	2.6×10^{-8} g/mL	1 h	[37]
Immunity	AFP	5×10^{-8}-1×10^{-5} g/mL	5×10^{-9} g/mL	2 h	[38]
SERS microarray chip	hnRNP A1	10^{-12} –10^{-6} g/mL	6.2×10^{-12} g/mL	15 min	This work
	S100P	10^{-12} –10^{-6} g/mL	6.51×10^{-12} g/mL		

grade intraepithelial neoplasia in the rectal mucosa. Finally, Figure 7C, F, and I show a bulging, inflammatory-type lesion in the ascending colon, with deep infiltration. Pathological diagnosis confirmed colorectal cancer.

Analysis of Clinical Samples

Figure 8A displays the physical image of the SERS integrated microarray chip. Using this chip, we conducted SERS assays on 90 serum clinical samples, collecting average spectra from both healthy individuals and patients (Figure 8B).

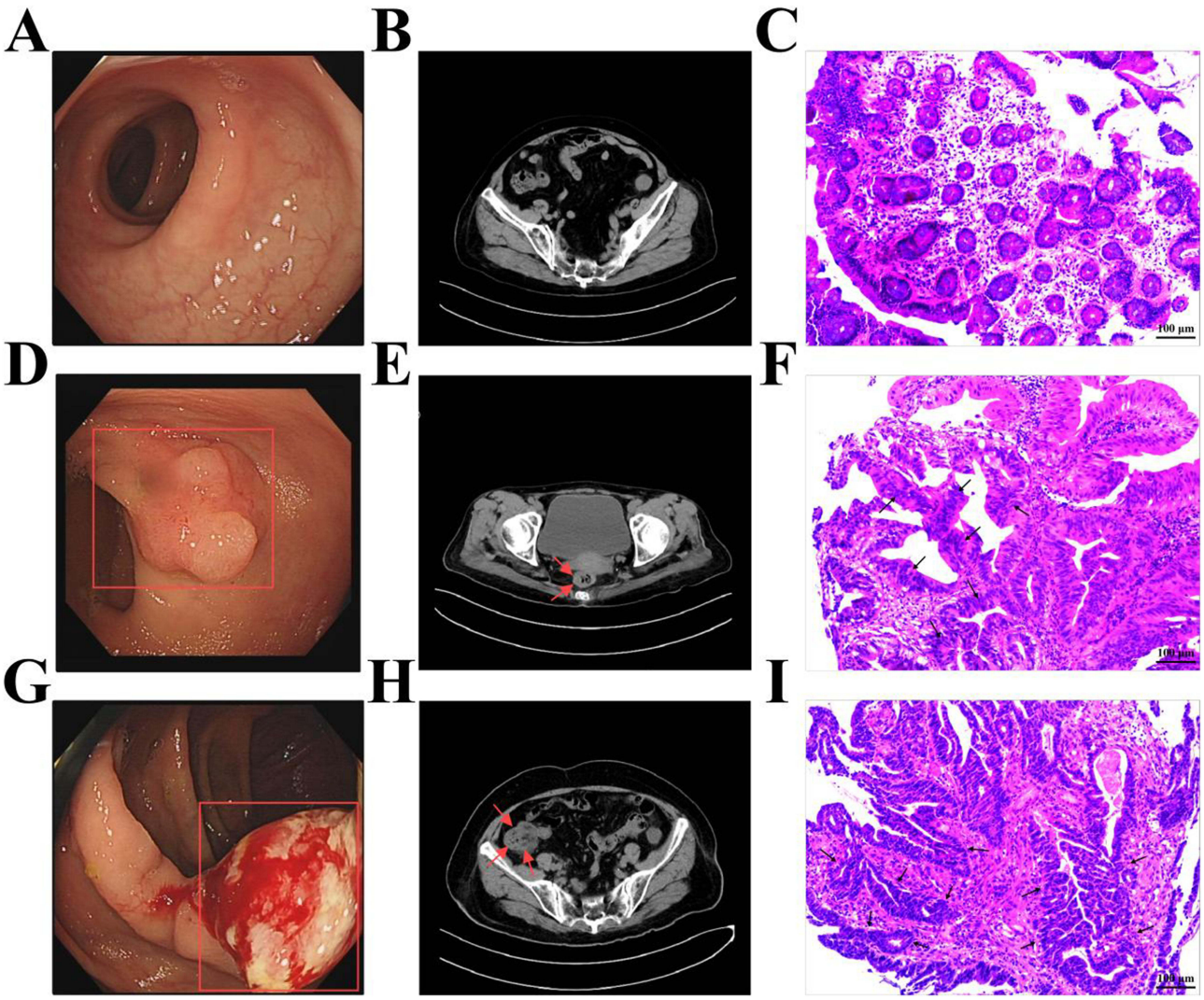

Figure 7 (**A-C**) Enteroscopic images, CT and HE staining of pathologic sections of a normal sigmoid colon. (**D-F**) Enteroscopic images, CT and HE staining of pathologic sections of colorectal precancerous lesions. (**G-I**) Confirmation of the diagnosis of colorectal cancer by colonoscopic images, CT and HE staining of pathologic sections.

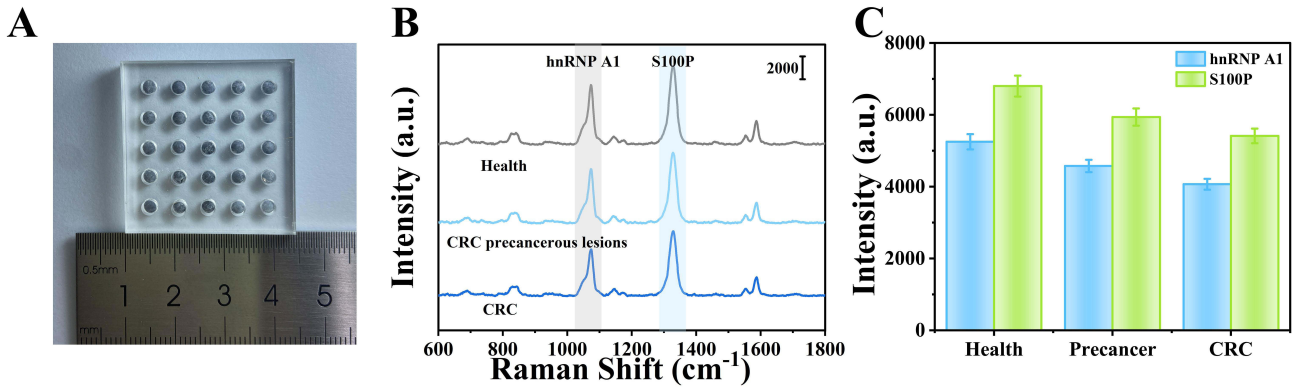

Figure 8 (**A**) Physical image of SERS integrated microarray chip. (**B**) Average serum SERS spectra of 30 healthy subjects, 30 patients with colorectal pre-cancer and 30 CRC patients. (**C**) Histogram of SERS intensity corresponding to the characteristic peaks at 1073 cm^{-1} (hnRNP A1) and 1330 cm^{-1} (S100P).

Histograms of SERS intensity for the characteristic peaks at 1073 cm^{-1} and 1330 cm^{-1} are shown in Figure 8C. The SERS intensities at these peaks were applied to the corresponding linear regression equations to calculate the expression levels of hnRNP A1 and S100P in the clinical serum samples (Figure 6B and C). The experimental results were compared to ELISA results (Tables S2–S4), demonstrating that hnRNP A1 and S100P expression levels were progressively higher in patients with precancerous lesions and CRC than in healthy individuals. As presented in Table 3, the results of the SERS integrated microarray platform were highly consistent with those of ELISA. Therefore, this platform is capable of accurately detecting hnRNP A1 and S100P in clinical serum samples, providing valuable support for the diagnosis and detection of precancerous lesions in the colon and rectum.

Conclusion and Discussion

In summary, this study presents a rapid and accurate analytical platform for the clinical detection of tumor markers by integrating innovative SERS technology with an aptamer recognition-release strategy. The high-throughput microarray chip, combined with Au/SnO_2 NRAs, enables the sensitive recognition and efficient detection of hnRNP A1 and S100P in serum samples, with a detection time of only 15 minutes. The Au/SnO_2 NRAs demonstrated exceptional SERS activity due to their highly ordered and closely packed ring structure, allowing for the detection of tumor markers at extremely low concentrations, with detection limits of 6.2×10^{-12} g/mL for hnRNP A1 and 6.51×10^{-12} g/mL for S100P. The SERS analytical platform also showed excellent stability, specificity, and reproducibility, providing valuable technical support for the early detection, timely intervention, and treatment of CRC. When compared to the classic ELISA assay, the results obtained from the SERS platform were accurate and reliable, further highlighting its potential for clinical applications. This novel aptamer recognition-release strategy, coupled with a SERS microarray chip, demonstrates great promise for monitoring and evaluating CRC precancerous lesions. However, while the method shows excellent detection performance, there are still challenges to address. These include the complexity of data analysis, as well as limitations in

Table 3 Comparison of SERS and ELISA Results for Clinical Serum Samples

Sample	SERS (ng/mL)		ELISA (ng/mL)		RSD (%)		RE (%)	
	hnRNP A1	S100P	hnRNP A1	S100P	hnRNP A1	S100P	hnRNP A1	S100P
Health	39.10±2.23	16.05±1.02	40.77±2.05	16.94±1.28	5.70	6.35	4.27	5.55
Precancer	60.26±2.60	39.74±1.87	63.20±2.55	41.59±1.75	4.31	4.71	4.88	4.66
CRC	112.40±6.32	60.27±2.86	118.07±5.95	63.47±3.49	5.62	5.04	5.04	5.31

aptamer selection and validation. Future efforts should focus on optimizing these aspects to ensure the wider adoption of this technology in clinical diagnostics and treatment.

Data Sharing Statement

The data for this study can be obtained by the corresponding author (Xiaogang Qin, Email: tzqinxiaogang@163.com).

Funding

This work was supported by the Nantong Basic Research Project (JC22022033) and the Open Project of Key Research Institute of State Administration of Traditional Chinese Medicine (202256).

Disclosure

The authors declare that there are no conflicts of interest related to this article.

References

1. Collado M, Castillo M, de Mier GJ M, de la Pinta C, Pena C. The diet as a modulator of tumor microenvironment in colorectal cancer patients. *Int J Mol Sci*. 2023;24(8):7317. doi:10.3390/ijms24087317
2. He S, Zhou C, Peng H, Lin M. Recent advances in fecal gene detection for colorectal cancer diagnosis. *Biomarkers Med*. 2021;15(14):1299–1308. doi:10.2217/bmm-2021-0269
3. Pinheiro M, Moreira DN, Ghidini M. Colon and rectal cancer: an emergent public health problem. *World J Gastroenterol*. 2024;30(7):644–651. doi:10.3748/wjg.v30.i7.644
4. Ding M, Yan J, Chao G, Zhang S. Application of artificial intelligence in colorectal cancer screening by colonoscopy: future prospects (Review). *Oncol Rep*. 2023;50(5):199. doi:10.3892/or.2023.8636
5. Shen Y, Wang D, Yuan T, et al. Novel DNA methylation biomarkers in stool and blood for early detection of colorectal cancer and precancerous lesions. *Clin epigenetics*. 2023;15(1):26. doi:10.1186/s13148-023-01443-7
6. Kim CW, Kim H, Kim HR, et al. Colorectal cancer screening using a stool DNA-based SDC2 methylation test: a multicenter, prospective trial. *BMC Gastroenterol*. 2021;21(1):173. doi:10.1186/s12876-021-01759-9
7. Tepus M, Yau TO. Non-Invasive Colorectal Cancer Screening: an Overview. *Gastro Tumors*. 2020;7(3):62–73. doi:10.1159/000507701
8. Ma CX, Guan X, Wang S, Liu Z, Jiang Z, Wang XS. Application and prospect of fecal DNA test in colorectal cancer screening. *Zhonghua Wei Chang Wai Ke Za Zhi*. 2019;22(5):491–494. doi:10.3760/cma.j.issn.1671-0274.2019.05.018
9. Zhang Z, Zhang D, Cui Y, Qiu Y, Miao C, Lu X. Identification of microRNA-451a as a novel circulating biomarker for colorectal cancer diagnosis. *Biomed Res Int*. 2020;2020:5236236. doi:10.1155/2020/5236236
10. Urbiola-Salvador V, Jablonska A, Miroszewska D, et al. Plasma protein changes reflect colorectal cancer development and associated inflammation. *Front Oncol*. 2023;13:1158261. doi:10.3389/fonc.2023.1158261
11. Liu L, Huang Y, Li Y, et al. FJX1 as a candidate diagnostic and prognostic serum biomarker for colorectal cancer. *Clin Transl Oncol*. 2022;24(10):1964–1974. doi:10.1007/s12094-022-02852-5
12. Lee SH, Park YE, Lee JE, Lee HJ. A surface plasmon resonance biosensor in conjunction with a DNA aptamer-antibody bioreceptor pair for heterogeneous nuclear ribonucleoprotein A1 concentrations in colorectal cancer plasma solutions. *Biosens Bioelectron*. 2020;154:112065. doi:10.1016/j.bios.2020.112065
13. Shen Z-Y, Fang Y, Zhen L, et al. Analysis of the predictive efficiency of MOP on adverse prognosis and the pathogenesis of S100P-mediated invasion and metastasis of colon adenocarcinoma. *Cancer Gen*. 2016;209(4):143–153. doi:10.1016/j.cancergen.2016.02.002
14. Nedelkov D. Mass spectrometry-based immunoassays for the next phase of clinical applications. *Expert Rev Proteomics*. 2006;3(6):631–640. doi:10.1586/14789450.3.6.631
15. Hussaini HM, Seo B, Rich AM. Immunohistochemistry and immunofluorescence. *Methods Mol Biol*. 2023;2588:439–450.
16. Lengfeld J, Zhang H, Stoesz S, et al. Challenges in detection of serum oncoprotein: relevance to breast cancer diagnostics. *Breast Cancer Targets Ther*. 2021;13:575–593. doi:10.2147/BCTT.S331844
17. Gao Y, Wu Y, Huang P, Wu F-Y. Carbon dot-encapsulated plasmonic core-satellite nanoprobes for sensitive detection of cancer biomarkers via dual-mode colorimetric and fluorometric immunoassay. *ACS Appl Nano Mater*. 2022;5(8):11539–11548. doi:10.1021/acsanm.2c02554
18. Jin S, Zhang D, Yang B, Guo S, Chen L, Jung YM. Noble metal-free SERS: mechanisms and applications. *Analyst*. 2023;149(1):11–28. doi:10.1039/D3AN01669B
19. Cao Y, Zhang J, Yang Y, Huang Z, Nguyen Viet L, Fu C. Engineering of SERS substrates based on noble metal nanomaterials for chemical and biomedical applications. *Appl Spectrosc Rev*. 2015;50(6):499–525. doi:10.1080/05704928.2014.923901
20. Hu J, Zhang C. Surface-enhanced raman scattering technology and its application to gene analysis. *Progress in Chemistry*. 2010;22(8):1641–1647.
21. Zhang Y, Mi X, Tan X, Xiang R. Recent progress on liquid biopsy analysis using surface-enhanced raman spectroscopy. *Theranostics*. 2019;9(2):491–525. doi:10.7150/thno.29875
22. Hu W, Xia L, Hu Y, Li G. Recent progress on three-dimensional substrates for surface-enhanced raman spectroscopic analysis. *Microchem J*. 2022;172:106908. doi:10.1016/j.microc.2021.106908
23. Yan M, Li H, Li M, Cao X, She Y, Chen Z. Advances in surface-enhanced raman scattering-based aptasensors for food safety detection. *J Agricult Food Chemistry*. 2021;69(47):14049–14064. doi:10.1021/acs.jafc.1c05274
24. Wang H-X, Zhao Y-W, Li Z, Liu B-S, Zhang D. Development and application of aptamer-based surface-enhanced raman spectroscopy sensors in quantitative analysis and biotherapy. *Sensors*. 2019;19(17):3806. doi:10.3390/s19173806

25. Hu C, Shen J, Yan J, et al. Highly narrow nanogap-containing Au@Au core-shell SERS nanoparticles: size-dependent Raman enhancement and applications in cancer cell imaging. *Nanoscale*. 2016;8(4):2090–2096. doi:10.1039/C5NR06919J
26. Celik M, Altuntas S, Buyukserin F. Fabrication of nanocrater-decorated anodic aluminum oxide membranes as substrates for reproducibly enhanced SERS signals. *Sens Actuat B-Chem*. 2018;255:2871–2877. doi:10.1016/j.snb.2017.09.105
27. Beffara F, Perumal J, Mahyuddin AP, et al. Development of highly reliable SERS-active photonic crystal fiber probe and its application in the detection of ovarian cancer biomarker in cyst fluid. *J Biophotonics*. 2020;13(3):e201960120. doi:10.1002/jbio.201960120
28. Zhang Z, Yu L, Xu L, et al. Biotoxin sensing in food and environment via microchip. *Electrophoresis*. 2014;35(11):1547–1559. doi:10.1002/elps.201300570
29. Situma C, Hashimoto M, Soper SA. Merging microfluidics with microarray-based bioassays. *Biomol. Eng*. 2006;23(5):213–231. doi:10.1016/j.bioeng.2006.03.002
30. Chen X, Yao C, Li Z. Microarray-based chemical sensors and biosensors: fundamentals and food safety applications. *Trac-Trends Anal Chem*. 2023;158:116785. doi:10.1016/j.trac.2022.116785
31. Qu X, Lin R, Chen H. Microfluidic chip based microarray analysis. *Progress in Chemistry*. 2011;23(1):221–230.
32. Lee S, Dang H, Moon J-I, et al. SERS-based microdevices for use as in vitro diagnostic biosensors. *Chem Soc Rev*. 2024;53(11):d3cs01055d.
33. Hong KY, Brolo AG. Polarization-dependent surface-enhanced raman scattering (SERS) from microarrays. *Anal Chim Acta*. 2017;972:73–80. doi:10.1016/j.aca.2017.04.003
34. Chen S, Guo Z, Sang DK, et al. Gold-patterned microarray chips for ultrasensitive surface-enhanced Raman scattering detection of ultratrace samples. *J Raman Spectroscopy*. 2019;50(1):26–33. doi:10.1002/jrs.5506
35. Le Ru EC, Auguie B. Enhancement factors: a central concept during 50 years of surface-enhanced raman spectroscopy. *Acs Nano*. 2024;18(14):9773–9783. doi:10.1021/acsnano.4c01474
36. Wang Q-L, Cui H-F, C-L L, Song X, Q-Y L, Z-Y L. A multimode aptasensor based on hollow gold nanoparticles and structure switching of aptamer: fast and sensitive detection of carcinoembryonic antigen. *Sens Actuators Rep*. 2020;2(1):100021. doi:10.1016/j.snr.2020.100021
37. Chen Y, Yang Y, Xie Q, Lai Q, Ji X, He Z. Homogeneous immunoassay for alpha-fetoprotein based on the quenching of the fluorescence of quantum dots by antibody labelled with complexed copper ion tags. *Mikrochim Acta*. 2020;187(4):252. doi:10.1007/s00604-020-04229-3
38. Zhang C, Gao Y, Yang N, You T, Chen H, Yin P. Direct determination of the tumor marker AFP via silver nanoparticle enhanced SERS and AFP-modified gold nanoparticles as capturing substrate. *Mikrochim Acta*. 2018;185(2):90. doi:10.1007/s00604-017-2652-y